Acta Crystallographica Section F
Structural Biology and Crystallization Communications
ISSN 1744-3091

Purification, crystallization, small-angle X-ray scattering and preliminary X-ray diffraction analysis of the SH2 domain of the Csk-homologous kinase

Natalie J. Gunn,[a] Michael A. Gorman,[b] Renwick C. J. Dobson,[a,c] Michael W. Parker[a,b] and Terrence D. Mulhern[a]*

[a]Department of Biochemistry and Molecular Biology, Bio21 Molecular Science and Biotechnology Institute, University of Melbourne, 30 Flemington Road, Parkville, Victoria 3010, Australia, [b]Biota Structural Biology Laboratory, St Vincent's Institute of Medical Research, 9 Princes Street, Fitzroy, Victoria 3065, Australia, and [c]The Biomolecular Interactions Centre, School of Biological Sciences, University of Canterbury, Private Bag 4800, Christchurch, New Zealand

Correspondence e-mail: tmulhern@unimelb.edu.au

Received 25 November 2010
Accepted 22 December 2010

The C-terminal Src kinase (Csk) and Csk-homologous kinase (CHK) are endogenous inhibitors of the proto-oncogenic Src family of protein tyrosine kinases (SFKs). Phosphotyrosyl peptide binding to their Src-homology 2 (SH2) domains activates Csk and CHK, enhancing their ability to suppress SFK signalling; however, the detailed mechanistic basis of this activation event is unclear. The CHK SH2 was expressed in *Escherichia coli* and the purified protein was characterized as monomeric by synchrotron small-angle X-ray scattering in-line with size-exclusion chromatography. The CHK SH2 crystallized in 0.2 *M* sodium bromide, 0.1 *M* bis-Tris propane pH 6.5 and 20% polyethylene glycol 3350 and the best crystals diffracted to ∼1.6 Å resolution. The crystals belonged to space group *P*2, with unit-cell parameters a = 25.8, b = 34.6, c = 63.2 Å, β = 99.4°.

1. Introduction

In mammals, two Csk-family protein tyrosine kinases, C-terminal Src kinase (Csk) and Csk-homologous kinase (CHK), specifically phosphorylate the C-terminal regulatory site of the Src-family kinases (SFKs; c-Src, Blk, Fgr, Fyn, Hck, Lck, Lyn and Yes; reviewed in Chong, Ia *et al.*, 2005; Chong, Mulhern *et al.*, 2005). C-terminal tail phosphorylation of SFKs favours their 'closed' inactive state, thereby attenuating SFK signalling (Sicheri *et al.*, 1997; Xu *et al.*, 1997). The Csk-family kinases themselves are activated by phosphotyrosyl ligand binding by their Src-homology 2 (SH2) domains, thereby enhancing their ability to inhibit SFK signalling (Zrihan-Licht *et al.*, 1997, 1998; Takeuchi *et al.*, 2000; Ayrapetov *et al.*, 2005). As the SFKs are known proto-oncogenes that mediate proliferative responses downstream of numerous cell-surface receptors (Hunter, 1995; Pawson, 2004), it is important to understand the mechanistic basis of Csk and CHK activation and whether this could be exploited in the design of therapeutic inhibitors of SFK signalling.

The structure of full-length Csk has been determined (Ogawa *et al.*, 2002) and as CHK shares 53% sequence identity with Csk it is likely that they share a similar three-dimensional structure. The crystal structure of Csk revealed that both the SH3 and SH2 domains make contact with the N-terminal lobe of the kinase domain, which suggests that these domains and the SH3–SH2 linker might be involved in regulation of kinase activity. There were six Csk conformers in the asymmetric unit: four active conformers and two inactive conformers based upon the position of their respective catalytic α-helix *C* (Ogawa *et al.*, 2002). A major difference between these putative active and inactive structures was the orientation of their SH2 domain. In the active state the SH2 domain makes contacts with the loop preceding α-helix *C*, while in the inactive conformation the SH2 domain is rotated 60° upwards with respect to the kinase domain, breaking these contacts. The binding of SH2 ligands has been shown to activate Csk and CHK (Zrihan-Licht *et al.*, 1997, 1998; Takeuchi *et al.*, 2000; Ayrapetov *et al.*, 2005), presumably by stabilizing the SH2–kinase domain contacts, but how the effect of SH2 ligand binding is propagated to the kinase domain is still unclear.

As a first step in investigating the mechanism of CHK activation, we present here the preliminary small-angle X-ray scattering, crystallization and X-ray diffraction analysis of the SH2 domain of CHK.

These and subsequent studies of the effect of ligand binding to the SH2 domain are likely to provide insight into the mechanism of catalytic regulation of CHK and Csk.

2. Materials and methods

2.1. Gene synthesis

The coding sequence corresponding to residues 71–174 of *Rattus norvegicus* CHK (UniProt P41243) was optimized for *Escherichia coli* expression (OptimumGene algorithm, GenScript), synthesized with flanking 5′ *Nde*I and 3′ *Xho*I sites and subcloned into the pGS21a expression vector (Genscript). The expressed protein corresponds to the native amino-acid sequence with the addition of an N-terminal Met. These sequence boundaries were selected based on analysis of NMR NOE, *J* couplings and chemical shift data recorded on a longer (residues 69–186) rat CHK SH2 construct (Mulhern *et al.*, 2002). DNA was transformed into DH5α *E. coli* and grown overnight in a 5 ml culture. Purified DNA was prepared using a QIAprep Spin Miniprep Kit (Qiagen) and transformed into BL21 *E. coli* for protein expression.

2.2. Expression and purification

Transformed cells were grown in 2–3 l Luria–Bertani broth with 0.1 mg ml^{-1} ampicillin at 310 K until they reached an OD_{600} of 0.6–0.9. IPTG was added to 1 m*M* and protein was expressed for 3–4 h. Cells were harvested by centrifugation at 2990*g* for 20 min at 277 K. The cell pellet was either stored at 253 K or lysed immediately. Prior to lysis, the cell pellet was resuspended in 20 m*M* HEPES pH 8.0, 50 m*M* NaCl, 1 m*M* DTT and EDTA-free protease-inhibitor cocktail (Roche). Cell lysis was performed by sonication on ice (5 s bursts, 15 s rests) using an MSE Soniprep 150 sonicator. The insoluble fraction was removed by centrifugation at 27 000*g* for 45 min at 277 K. The soluble fraction was filtered through a 0.45 µm PVDF filter and was then subjected to phosphotyrosine affinity chromatography on 5 ml *o*-phospho-L-tyrosine agarose (Sigma) pre-equilibrated in buffer *A* (20 m*M* HEPES pH 8.0, 50 m*M* NaCl and 1 m*M* DTT). Batch binding was performed for 1–4 h at 277 K with gentle rocking. The resin was then washed with 10 column volumes (CV) buffer *A*. The bound protein was eluted with 10 CV buffer *B* (20 m*M* HEPES pH 8.0, 1 *M* NaCl and 1 m*M* DTT). Fractions were analysed using SDS–PAGE and the CHK SH2-containing fractions were pooled, concentrated and subjected to size-exclusion chromatography. Typically, 10–30 mg protein was loaded onto a Superdex 200 10/300 gel-filtration column (GE Healthcare) equilibrated in buffer *C* (10 m*M* HEPES pH 8.0, 1 m*M* DTT). Fractions containing the CHK SH2 domain were pooled and concentrated in preparation for small-angle X-ray scattering analysis and crystallization.

2.3. Small-angle X-ray scattering

Small-angle X-ray scattering (SAXS) data were collected at the Australian Synchrotron on the SAXS/WAXS beamline. The X-ray beam size at the sample was 250 µm horizontal × 80 µm vertical and data were collected using a Pilatus 1M detector positioned 900 mm from the sample, giving a q range of 0.01–0.6 Å^{-1} where q is the magnitude of the momentum-transfer vector and $q = (4\pi\sin\theta)/\lambda$, where the scattering angle is 2θ and λ is the X-ray wavelength (1.0332 Å). The protein sample analysed was subjected to in-line size-exclusion chromatography on a Superdex 200 5/150 GL gel-filtration column (GE Healthcare) with a bed volume of 3 ml equilibrated with buffer *C* at a flow rate of 0.2 ml min^{-1}. 50 µl CHK SH2 at 11 mg ml^{-1} was injected and the fractionated sample flowed through a 1.5 mm quartz capillary where it was exposed to the X-ray beam. 600 detector images of sequential 2 s exposures (2.1 s repeat time) were collected at 298 K, corresponding to a total elution volume of 4.2 ml. Radial averaging, background subtraction and image-series analysis were performed using *SAXS*15*ID* software (Australian Synchrotron). Five sequential detector images were averaged to generate each SAXS data set for subsequent analysis using the *ATSAS* (v.2.3) software (Konarev *et al.*, 2006).

Table 1
X-ray data-collection statistics.

Values in parentheses are for the highest resolution shell. The Matthews coefficient and the estimate of the solvent content are based on a molecular weight of 12 222.2 Da in the asymmetric unit (one molecule of CHK SH2 of 12 222.2 Da).

Wavelength (Å)	0.95369
No. of images	210
Oscillation (°)	1
Space group	*P*2
Unit-cell parameters (Å, °)	a = 25.8, b = 34.4, c = 62.3, β = 99.4
Resolution (Å)	20.78–1.54 (1.64–1.54)
Observed reflections	63990 (9264)
Unique reflections	16040 (2544)
Completeness (%)	98.5 (97.8)
$R_{\rm merge}$†	0.130 (0.554)
$R_{\rm meas}$	0.093 (0.536)
Mean $I/\sigma(I)$	11.94 (3.08)
Multiplicity	3.98 (3.64)
Estimated molecules per asymmetric unit	1
$V_{\rm M}$ (Å^3 Da^{-1})	2.28
Solvent content (%)	46

† $R_{\rm merge} = \sum_{hkl}\sum_i |I_i(hkl) - \langle I(hkl)\rangle| / \sum_{hkl}\sum_i I_i(hkl)$.

2.4. Crystallization

Purified CHK SH2 at 10 mg ml^{-1} in buffer *C* was subjected to initial screening by sitting-drop vapour diffusion at the C^3 Collaborative Crystallization Centre, CSIRO Parkville, Australia (http://www.csiro.au/c3/) using the JCSG+ and PACT screens (Qiagen) at 281 and 293 K (Newman *et al.*, 2005, 2008). Drops consisted of 100 nl protein solution in buffer *C* and 100 nl reservoir solution. Crystals began to form as thin plates after 5 d at 281 K. In-house optimization using the hanging-drop vapour-diffusion method determined reproducible crystallization conditions using the high-molecular-weight polyethylene glycol precipitants PEG 3350 and PEG 6000 and a slightly acidic pH. The crystals from which diffraction data were collected were obtained using 100 nl protein solution in buffer *C* and 100 nl 0.2 *M* sodium bromide, 0.1 *M* bis-Tris propane pH 6.5, 20%(*w*/*v*) PEG 3350 with 0.02%(*w*/*v*) sodium azide as an antimicrobial agent. Crystals also formed in a condition containing PEG 1500, but as this condition also contained phosphate, which is known to bind in the phosphotyrosyl-binding pocket of SH2 domains, further optimization of this condition was not carried out.

2.5. Data collection and processing

Diffraction data were collected on the microfocus macromolecular crystallography (MX2) beamline at the Australian Synchrotron using an ADSC Q315R detector positioned 200 mm from the crystal with the *Blu-Ice* software (McPhillips *et al.*, 2002). The crystal was removed from the drop using a 0.1 mm loop and placed in a drop containing mother liquor and 50% glycerol. The crystal was then flash-cooled in liquid nitrogen and intensity data were collected at 100 K. 210° of data were collected with 1° rotation and 2 s exposure. Data were indexed, integrated and scaled using *XDS* (Kabsch, 2010). Molecular replacement was conducted using *Phaser* (McCoy *et al.*,

2007) and model refinement was conducted using *REFMAC*5 (Murshudov *et al.*, 1997) from *CCP*4 (Collaborative Computational Project, Number 4, 1994). Model building was performed using *Coot* (Emsley & Cowtan, 2004). Data-collection statistics are given in Table 1.

3. Results and discussion

Recombinant CHK SH2 was expressed in *E. coli* and purified by phosphotyrosine affinity and size-exclusion chromatography. The purity of the sample was determined using SDS–PAGE (Fig. 1) and it was estimated to be >95% pure. The yield for this purification was 20 mg per litre of cell culture. The purified protein was subjected to synchrotron SAXS analysis in-line with size-exclusion chromatography (Fig. 2). The CHK SH2 protein eluted as a single peak with a consistent radius of gyration (R_g). The R_g for the averaged SAXS data was 15.02 ± 0.45 Å as calculated by *AUTORG* (Konarev *et al.*, 2006). Estimation of the mass of the scattering particle using *AUTOPOROD* (Konarev *et al.*, 2006) gave 12.3 ± 0.5 kDa, which is in excellent agreement with the expected monomer mass of 12.2 kDa. The experimental SAXS profile of CHK SH2 was compared with the theoretical scattering profile generated from the Csk SH2 coordinates (PDB entry 3eac; D. Liu, R. D. Seidel & D. Cowburn, unpublished work) using *CRYSOL* (Svergun *et al.*, 1995). The goodness of fit of the theoretical curve was excellent, with a reduced χ^2 statistic (χ^2_ν) of 0.911 over $N = 746$ data points, which gives $P(\chi; \nu) = 0.957$ (Mills *et al.*, 2009). Thus, SAXS analysis of the purified protein indicated that it was homogeneous and monomeric, with a very similar overall structure to the Csk SH2.

Initial screening of crystallization conditions was performed as described in §2.4. Crystals formed predominantly in high-molecular-weight PEG and at slightly acidic pH as thin plates that seeded off the surface of the plate. To date, crystals have only been obtained at a temperature of 281 K. Long thin needle-like crystals were obtained at an initial protein concentration of 15 mg ml^{-1}. Larger crystals (300 × 30 × 5 µm) were obtained by decreasing the protein concentration to 10 mg ml^{-1} in the same conditions. The crystal marked with an asterisk in Fig. 3 was removed from the drop and briefly soaked in cryoprotectant before being flash-frozen in liquid nitrogen.

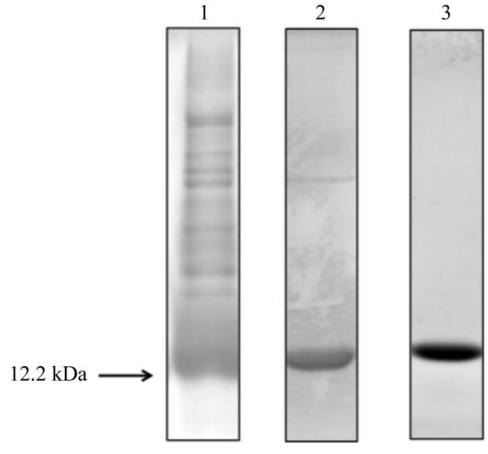

Figure 1
14% SDS–PAGE was used to assess the purity of the recombinant protein. Lane 1, soluble fraction obtained following cell lysis. Lane 2, pooled eluate fractions following phosphotyrosine agarose affinity liquid chromatography. Lane 3, Superdex 200 (24 ml bed volume) pooled fractions.

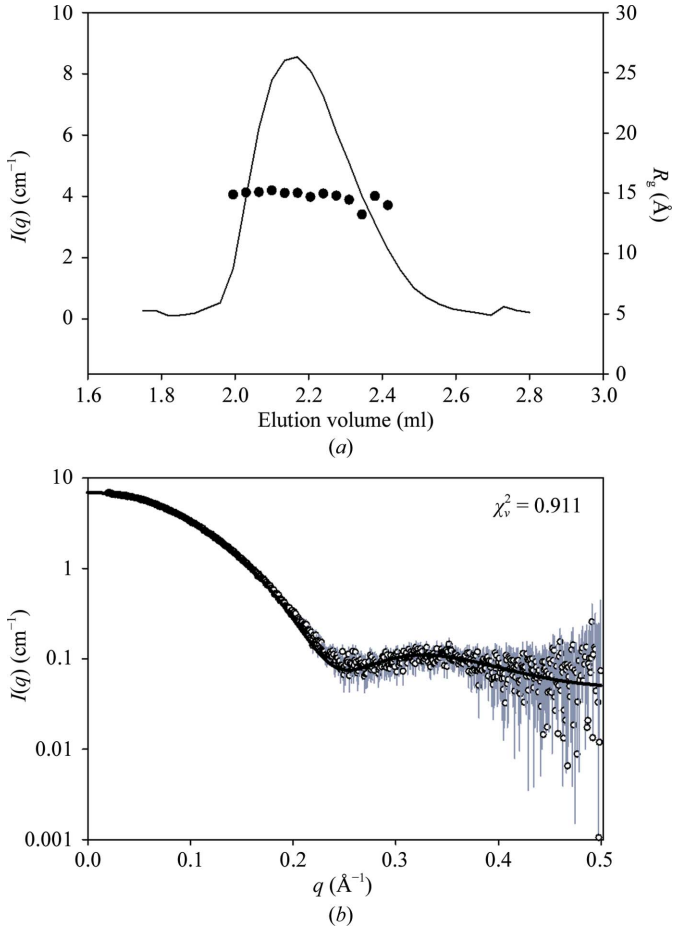

Figure 2
In-line SAXS analysis of size-exclusion fractionated CHK SH2. Purified CHK SH2 was subjected to size-exclusion chromatography on Superdex 200 (3 ml bed volume). (*a*) The scattering intensity at zero angle [$I(0)$] as a function of elution volume is shown by the solid line. The radius of gyration of the scattering particles, calculated by Guinier analysis, is shown as filled circles. (*b*) Comparison of the experimental CHK SH2 SAXS data with the theoretical scattering profile of the Csk SH2. The mean scattering intensity at each q value from the material eluted from 2.03 to 2.24 ml is shown as open circles and the error bars represent ± one standard deviation. The theoretical scattering profile calculated from the coordinates of the CsK SH2 (PDB entry 3eac) is shown as a solid line. The reduced χ^2 statistic (χ^2_ν) for the fit of the theoretical profile to the experimental data is indicated.

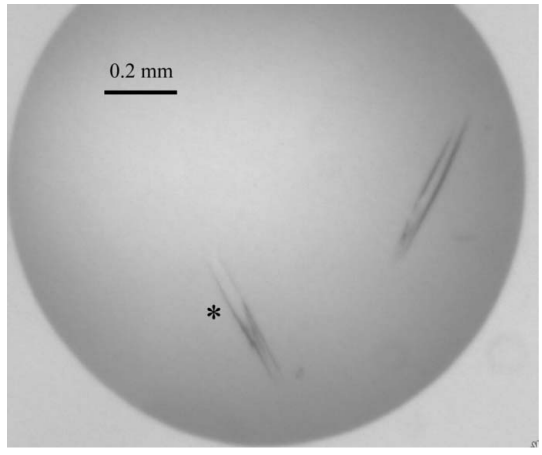

Figure 3
Crystals obtained using CHK SH2 at a concentration of 10 mg ml^{-1}.

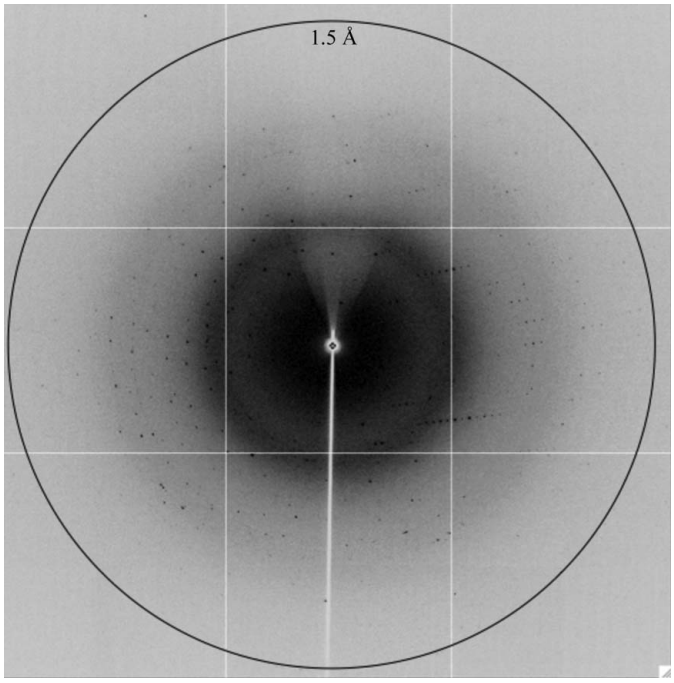

Figure 4
X-ray diffraction image obtained from the CHK SH2-domain crystal shown in Fig. 3. Diffraction was obtained to beyond 1.6 Å resolution. The oscillation range for this image is 1°.

Fig. 4 shows diffraction data collected from the crystal shown in Fig. 3. The crystal diffracted to 1.54 Å resolution and the space group was determined to be *P*2. The unit-cell parameters were a = 25.8, b = 34.4, c = 62.3 Å, β = 99.4°. V_M was calculated to be 2.28 Å^3 Da^{-1} assuming the presence of one molecule in the asymmetric unit, which corresponds to a solvent content of 46% (Matthews, 1968). Molecular replacement (together with rigid-body refinement) was successfully performed using residues Lys76–Met173 of the human Csk SH2 domain (PDB entry 3eac; 56% identity, LL gain = 304.5, Z score = 10.5; R_{init} = 48%). This initial solution produced R-factor and R_{free} values of 29.9% and 42.5%, respectively. The electron-density maps produced were of sufficient quality to allow placement of the correct sequence. The current model has been refined to R-factor and R_{free} values of 17.2% and 20.5%, respectively. The presence of phosphate in the phosphotyrosine-binding pocket of other SH2 domains has been shown to stabilize a conformation similar to that observed when a phosphopeptide is bound (Lange *et al.*, 2003). Thus far, no additional density has been observed in the phosphotyrosine-binding pocket, suggesting that this structure represents the ligand-free state of the CHK SH2. We are currently attempting to crystallize the ligand-bound state of the CHK SH2 and anticipate that comparison of the ligand-free and ligand-bound structures will provide new insights into the mechanism by which CHK is regulated.

We would like to acknowledge the support and assistance of the staff at the Bio21 Collaborative Crystallographic Centre at CSIRO Molecular and Health Technologies, Parkville, Melbourne. This research was undertaken on the MX2 and SAXS/WAXS beamlines at the Australian Synchrotron, Victoria, Australia; we would like to thank Tom Caradoc-Davies and Nigel Kirby, respectively, for helpful discussion and assistance at the Australian Synchrotron. This work was supported by Australian National Health and Medical Research Council (NHMRC) Project Grant 509115 and Australian Institute of Nuclear Science and Engineering (AINSE) Award 09137 to TDM. RCJD acknowledges the C. R. Roper Fellowship for support. MWP is an Australian Research Council Federation Fellow and NHMRC Honorary Fellow.

References

Ayrapetov, M. K., Nam, N. H., Ye, G., Kumar, A., Parang, K. & Sun, G. (2005). *J. Biol. Chem.* **280**, 25780–25787.
Chong, Y.-P., Ia, K. K., Mulhern, T. D. & Cheng, H.-C. (2005). *Biochim. Biophys. Acta*, **1754**, 210–220.
Chong, Y.-P., Mulhern, T. D. & Cheng, H.-C. (2005). *Growth Factors*, **23**, 233–244.
Collaborative Computational Project, Number 4 (1994). *Acta Cryst.* D**50**, 760–763.
Emsley, P. & Cowtan, K. (2004). *Acta Cryst.* D**60**, 2126–2132.
Hunter, T. (1995). *Cell*, **80**, 225–236.
Kabsch, W. (2010). *Acta Cryst.* D**66**, 125–132.
Konarev, P. V., Petoukhov, M. V., Volkov, V. V. & Svergun, D. I. (2006). *J. Appl. Cryst.* **39**, 277–286.
Lange, G., Lesuisse, D., Deprez, P., Schoot, B., Loenze, P., Bénard, D., Marquette, J. P., Broto, P., Sarubbi, E. & Mandine, E. (2003). *J. Med. Chem.* **46**, 5184–5195.
Matthews, B. W. (1968). *J. Mol. Biol.* **33**, 491–497.
McCoy, A. J., Grosse-Kunstleve, R. W., Adams, P. D., Winn, M. D., Storoni, L. C. & Read, R. J. (2007). *J. Appl. Cryst.* **40**, 658–674.
McPhillips, T. M., McPhillips, S. E., Chiu, H.-J., Cohen, A. E., Deacon, A. M., Ellis, P. J., Garman, E., Gonzalez, A., Sauter, N. K., Phizackerley, R. P., Soltis, S. M. & Kuhn, P. (2002). *J. Synchrotron Rad.* **9**, 401–406.
Mills, R. D., Trewhella, J., Qiu, T. W., Welte, T., Ryan, T. M., Hanley, T., Knott, R. B., Lithgow, T. & Mulhern, T. D. (2009). *J. Mol. Biol.* **388**, 1043–1058.
Mulhern, T. D., To, C. & Cheng, H.-C. (2002). *J. Biomol. NMR*, **24**, 363–364.
Murshudov, G. N., Vagin, A. A. & Dodson, E. J. (1997). *Acta Cryst.* D**53**, 240–255.
Newman, J., Egan, D., Walter, T. S., Meged, R., Berry, I., Ben Jelloul, M., Sussman, J. L., Stuart, D. I. & Perrakis, A. (2005). *Acta Cryst.* D**61**, 1426–1431.
Newman, J., Pham, T. M. & Peat, T. S. (2008). *Acta Cryst.* F**64**, 991–996.
Ogawa, A., Takayama, Y., Sakai, H., Chong, K. T., Takeuchi, S., Nakagawa, A., Nada, S., Okada, M. & Tsukihara, T. (2002). *J. Biol. Chem.* **277**, 14351–14354.
Pawson, T. (2004). *Cell*, **116**, 191–203.
Sicheri, F., Moarefi, I. & Kuriyan, J. (1997). *Nature (London)*, **385**, 602–609.
Svergun, D., Barberato, C. & Koch, M. H. J. (1995). *J. Appl. Cryst.* **28**, 768–773.
Takeuchi, S., Takayama, Y., Ogawa, A., Tamura, K. & Okada, M. (2000). *J. Biol. Chem.* **275**, 29183–29186.
Xu, W., Harrison, S. C. & Eck, M. J. (1997). *Nature (London)*, **385**, 595–602.
Zrihan-Licht, S., Deng, B., Yarden, Y., McShan, G., Keydar, I. & Avraham, H. (1998). *J. Biol. Chem.* **273**, 4065–4072.
Zrihan-Licht, S., Lim, J., Keydar, I., Sliwkowski, M. X., Groopman, J. E. & Avraham, H. (1997). *J. Biol. Chem.* **272**, 1856–1863.